biomedicines

MDPI

Article

RETRACTED: ATT-Myc Transgenic Mouse Model and Gene Expression Identify Genotoxic and Non-Genotoxic Chemicals That Accelerating Liver Tumor Growth in Short-Term Toxicity

Mahmoud Elalfy [1,*], Ahmed Jaafar Aljazzar [2] and Mona G. Elhadidy [3,4]

[1] Clinical Science Department, College of Veterinary Medicine, King Faisal University, Al-Ahsa 3959-36362, Saudi Arabia
[2] Pathology Department, College of Veterinary Medicine, King Faisal University, Al-Ahsa 3959-36362, Saudi Arabia
[3] Medical Physiology, Faculty of Medicine, Mansoura University, Mansoura City 35516, Egypt
[4] Medical Physiology, Faculty of Medicine, Al-Baha University, Alaqiq 65779-7738, Saudi Arabia
* Correspondence: malhefnawy@kfu.edu.sa

Abstract: Introduction: Diethyl nitrosamine (DEN), a known carcinogen, has been used for validating the RasH2 and P53 transgenic models in chemical testing and has been shown to enhance primary liver tumor growth in the ATT-Myc transgenic mouse model of liver cancer. **Material and Methods:** to better understand the mechanism of hepatocellular carcinoma acceleration following DEN, BHT and vehicles treatments in ATT-Myc, transgenic and non-transgenic, mice. We employed an exon array, RT-PCR, Western blotting, and IHC to investigate the complex interplay between the c-Myc transgene and other growth factors in treated mice versus control transgenic and non-transgenic mice. **Results:** Notably, DEN treatment induced a 12-fold increase in c-Myc expression compared to non-transgenic mice. Furthermore, tumor growth in the DEN group was strongly associated with increased proliferation of transformed or carcinogenic hepatocytes, as evidenced by proliferative cell nuclear antigen and bromodeoxyuridine expression. Internally, the loss of c-Met signaling, enriched transcription factors, and the diminished expression of antioxidants, such as superoxide dismutase (SOD1) and NRF2, further enhanced c-Myc-induced liver tumor growth as early as four months post-DEN treatment. **Discussion:** Extensive tumor growth was observed at 8.5 months, coinciding with the downregulation of tumor suppressors such as p53. In contrast, at these time points, ATT-Myc transgenic mice exhibited only dysplastic hepatocytes without tumor formation. Additionally, the antioxidant butylated hydroxytoluene maintained c-Met expression and did not promote liver tumor formation. **Conclusions:** the persistent upregulation of c-Myc in the ATT-Myc liver cancer model, at both the gene and protein levels following DEN treatment inhibited the ETS1 transcription factor, further exacerbating the decline of c-Met signaling, SOD1, and NRF2. These changes led to increased reactive oxygen species production and promoted rapid liver tumor growth.

Keywords: DEN; HCC; c-Met/HGF signaling; SOD1; NRF2; ATT-Myc transgenic mouse model of liver cancer

Academic Editors: Felipe Javier Chaves-Martinez and Elias Kouroumalis

Received: 14 January 2025
Revised: 27 February 2025
Accepted: 28 February 2025
Published: 18 March 2025
Retracted: 16 September 2026

Citation: Elalfy, M.; Aljazzar, A.J.; Elhadidy, M.G. RETRACTED: ATT-Myc Transgenic Mouse Model and Gene Expression Identify Genotoxic and Non-Genotoxic Chemicals That Accelerating Liver Tumor Growth in Short-Term Toxicity. *Biomedicines* **2025**, *13*, 743. https://doi.org/10.3390/biomedicines13030743

1. Introduction

Death rates from hepatocellular carcinoma (HCC) are rising globally, with particularly high incidences in developing countries [1]. Significant progress has been made in the systemic treatment of advanced HCC over the last decade [2], especially in studying the

This paper has been retracted. A retraction notice was published on 16 September 2026 in *Biomedicines* **2026**, *14*, 2085. https://doi.org/10.3390/biomedicines14092085

tumor immune microenvironment and predicting HCC outcomes [3]. However, not all patients with HCC respond well to recently developed treatment approaches, and many exhibit therapeutic resistance [4].

Chemicals are often classified as carcinogens based on the presence of hepatocellular tumors in rat livers, which has significant implications. There is now greater potential to integrate the scientific understanding of the etiology of these tumors into hazard characterization and dose–response assessments, aligning them with human relevance frameworks [5]. Diethylnitrosamine (DEN) is a mutagenic and genotoxic agent that causes DNA alterations and gene expression changes, leading to liver cancer in experimental wild-type or transgenic animal models [6]. The mechanisms of DEN-induced chemical carcinogenesis have provided additional insights [7] into preventive and protective mechanisms against DEN exposure [8,9], although some aspects remain controversial. Understanding the biology of liver tumors is crucial for developing therapeutic agents and improving patient survival following chemical or surgical treatment [10].

Cyto-truncated c-Met transgene expression provides resistance to apoptotic stimuli in vivo and establishes immortalized, non-transformed hepatocyte cell lines [11]. The loss of c-Met signaling in c-Met conditional knockout animals accelerates DEN-induced liver tumor formation due to the compensatory high expression of epidermal growth factor receptor (EGFR) [9]. Conversely, DEN accelerates liver tumor growth in a hepatocyte growth factor (HGF) transgenic mouse model via c-Met activation [12]. The c-Myc transcription factor (TF) is a well-known oncogene due to its critical role in cancer and stem cell maintenance. Many frequently occurring human malignancies, including breast, colon, stomach, and pancreatic cancers, involve dysregulated c-Myc expression. Several human malignancies are influenced by c-Myc through its regulation of genes involved in mitochondrial and ribosomal synthesis, as well as glucose and glutamine metabolism [13]. Although c-Myc is expressed in various tissue tumors, few studies have explored anti-c-Myc antibody therapy for HCC [14]. Additionally, the use of herbal extracts containing quercetin as an active component has been investigated for directly targeting c-Myc by reducing reactive oxygen species (ROS) production [15] or inhibiting the release of exosomes from tumor cells under hypoxic conditions [16].

The goal of this study was to investigate the complex interplay of growth factors that enhance liver tumor formation in a c-Myc model treated with DEN. This research could contribute to the development of more effective HCC management protocols and potentially improve the survival rate for individuals suffering from HCC.

2. Materials and Methods

2.1. Laboratory Animals, Transgenicity, and Treatment

The Guide for the Care and Use of Laboratory Animals, eighth edition, National Academies Press, was followed for animal treatment. The study was approved by the Animal Welfare Ethics Commission of Hannover, Germany (33.9-42502-04-08/1619), as well as by the ethical committee of King Faisal University (KFU-25-ETHIC53114). The ATT-Myc transgenic line (c-myc model under alpha 1 antitrypsin promotor) was previously described by Dalemans et al. [17]. The transgenic mouse strain was of the C57BL/6 background. PCR was performed using HotStarTaq DNA polymerase (Qiagen, Germantown, MD, USA). Annealing temperatures and cycle numbers are indicated in brackets after each primer pair. The transgene was verified by a PCR analysis of DNA extracted from tail biopsies using the following forward and reverse primers: forward primer: 5′-TCCTGTACCTCGTCCGATTC-3′; reverse primer: 5′-GTTGTGCTGGTGAG-TGGAGA-3′ (60 °C, 31 cycles) (see Figure 1). Chemical treatments—DEN, butylated hydroxytoluene (BHT), corn oil, and saline vehicle—including doses and exposure conditions, were described earlier [3–5]. BrdU

(Sigma-Aldrich, Burlington, NJ, USA) was injected once at 100 mg/kg two hours before sacrifice [8]. Mice were sacrificed at four different time points (4, 5.5, 7, and 8.5 months). Animals were euthanized using excess CO_2, and histopathological analysis was performed. The remaining animals were disposed of safely.

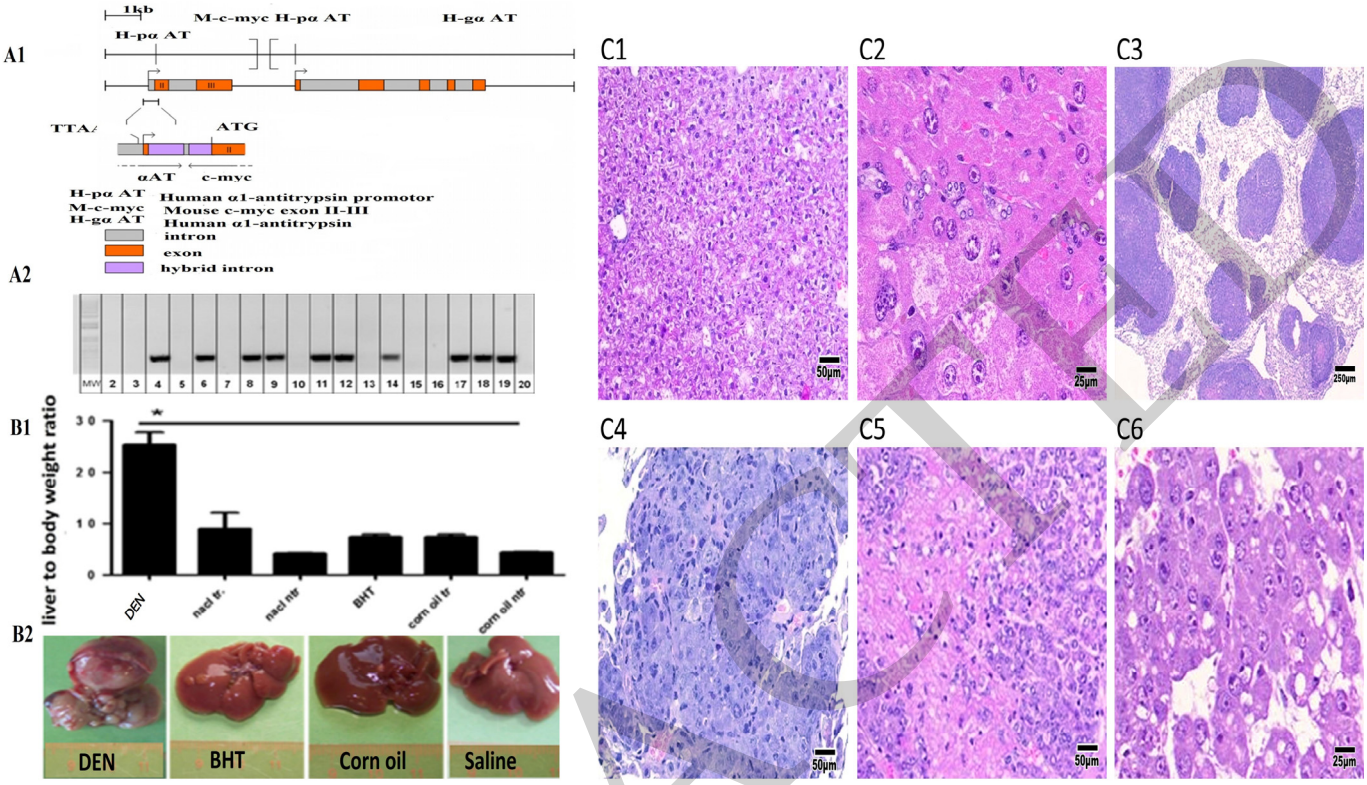

Figure 1. (**A1**,**A2**) ATT-Myc transgene construction and the positive band for transgenic ATT-Myc transgenes were confirmed by PCR tail DNA testing. (**B1**) The increase in liver weight to body weight ratio in DEN-treated transgenic mice at 8.5 months was due to massive liver tumor growth, as shown in the corresponding gross images. Moreover, these images illustrate a large liver in DEN-treated transgenic mice, small nodular structures in BHT-treated transgenic animals, and normal liver architecture in both transgenic and non-transgenic controls (**B2**). (**C1**) Histopathological analysis revealed that the normal liver parenchyma in non-transgenic mice remained unaltered. (**C2**) In BHT-treated transgenic animals, macrocytic dysplastic nodules were observed. (**C3**) illustrates liver cirrhosis and nodular regeneration in DEN-treated transgenic mice, large trabecular HCC, and pseudoglandular HCC (**C4**). Necrosis (**C5**) and fat changes (**C6**) were also detected. * $p < 0.05$.

2.2. Sample Collection and Preparation

Six mice were anesthetized using CO_2 overdose and sacrificed at 4, 5.5, 7, and 8.5 months. The thoracic cavity was opened using standard surgical procedures, and the liver was excised and rinsed with PBS. Organ weights were recorded, and tumors were inspected macroscopically before being separated from liver tissue. Liver samples were preserved in 4% buffered formalin or immediately frozen in liquid nitrogen.

2.3. Histology

Liver tissues from transgenic and control animals were fixed in 4% formaldehyde in PBS and embedded in paraffin following standard procedures. Paraffin-embedded tissues were sectioned into 3–5 μm slices and stained with hematoxylin and eosin (H&E).

2.4. Isolation of RNA from Liver Tissues and Exon Array Procedures and Analysis

NA was isolated from liver tissue as previously described Target Labeling Assay Manuals were strictly followed. The assay involved ribosomal RNA reduction, cDNA synthesis,

cRNA hydrolysis, fragmentation, terminal labeling, hybridization, washing, and staining of microarray chips. The sample preparation included RNA reduction and cDNA synthesis, purification of double-stranded cDNA, synthesis of biotin-labeled cRNA, purification of biotin-labeled cRNA, fragmentation of biotin-labeled cRNA, hybridization of GeneChip® arrays, washing and staining of GeneChip® arrays, and scanning of GeneChip® arrays.

2.5. Interpretation of GeneChip® Data

Quality indicators were assessed to determine the reliability of GeneChip® results. The GeneChip® Operating Software (Microarray. Suite 5.0 software) generated reports listing key expression ratios, including noise values (Q), target signal values, scale factors (SF), and hybridization controls. The software also provided normalized expression values for probe sets.

2.6. Validation of Gene Expression by Real Time-PCR (RT-PCR)

Total RNA was purified using QIAzol reagent (Qiagen, Germany). RNA quality was assessed using a Nanodrop 2000 spectrophotometer (Thermo Fisher Scientific, Waltham, MA, USA). cDNA synthesis was performed using reverse transcriptase enzyme (Bioline, London, UK). cDNA amplification was conducted using a real-time PCR machine (ThermoScientific, Waltham, MA, USA). The reaction volume was 20 µL. The PCR program was set at 95 °C for two minutes, followed by 40 cycles of denaturation at 95 °C for 10 s and annealing/extension at 60 °C for 30 s. The primer sequences used are listed in Table 1. β-actin was utilized as a reference gene. All experiments were performed in triplicate. Relative gene expression was calculated using the ΔCt method (Ct target gene—Ct housekeeping gene), and the $2-\Delta\Delta Ct$ method was utilized to determine fold changes (FCs) in gene expression. PCR products were imaged using a Kodak Image Station 440CF under UV light after agarose gel electrophoresis with ethidium bromide staining.

Table 1. Sequences of primers used in RT-PCR.

Primers: Forward (fw) and Reverse (rev)	Sequences	Product Size (bp)
Myc fw	TCCTGTACCTCGTCCGATTC	303
Myc rev	GTTGTGCTGGTGAGTGGAGA	
C9 fw	ATGGAGCAATTGGTCAGAGTG	241
C9 rev	ATCTCCACAGTCGTTGTCACC	
Nola2 fw	ATTGCCGATTGAGGTGTACTG	156
Nola2 rev	GCACTTGTCGTAGGTCTCCTG	
Bzw2 fw	CAGGCACTGAAGCACCTAAAG	194
Bzw2 rev	CACTTCAGTATCGCCTCTTCG	
Mmp12_2 fw	CCAGAGGTCAAGATGGATGAA	237
Mmp12_2 rev	TGGGCTAGTGTACCACCTTTG	

Table 1. *Cont.*

Primers: Forward (fw) and Reverse (rev)	Sequences	Product Size (bp)
Rpl13a fw	CTGCTGCTCTCAAGGTTGTTC	235
Rpl13a rev	TTGGTCTTGAGGACCTCTGTG	
Rfc4 fw	AGCCATGTCCTCCCTTTAAGA	223
Rfc4 rev	CCAGTAATCGCTCCTGTTGAA	
Dynll1 fw	GAAGAGATGCAACAGGACTCG	
Dynll1 rev	CCACCTGACCCAGGTAGAAGT	202
Slc10a1_fw	CACCATGGAGTTCAGCAAGAT	238
Slc10a1_rev	GGTCATCACAATGCTGAGGTT	
Gas6_fw	CGATGAATGCACAGACTCAGA	166
Gas6_rev	GTTGACACAGGTCTGCTCACA	
ß-Actin fw	GGCATTGTTACCAACTGGGACG	423
ß-Actin rev	CTCTTTGATGTCACGCACGATTTC	

2.7. Western Blotting

Frozen liver tissue samples were lysed in lysis buffer 3 supplemented with protease inhibitors (Benzonase). Whole-cell lysates were obtained by homogenization using an ultrasonic processor, followed by centrifugation at 10,000 rpm and 20 °C for 20 min. The supernatant was recovered, and the protein content of the lysate was determined using the Bradford protein assay (Bio-Rad), with bovine serum albumin as the standard.

A total of 100 µg of total protein extract was separated on 8%, 12%, and 15% SDS–polyacrylamide gels and subsequently blotted onto a PVDF membrane using 25 mM Tris and 190 mM glycine at 4 °C for two hours at 350 mA. Blots were blocked in Rotiblock (Roth, Karlsruhe, Germany) for one hour and then incubated with the primary antibodies listed in Table 2. After washing with Tris-buffered saline (25 mM Tris and 135 mM NaCl; pH 7.6) containing 0.1% Tween, the membranes were incubated with the corresponding secondary anti-mouse IgG κ antibody (sc-516102, Santa Cruz) at room temperature for one hour.

Table 2. List of antibodies used for Western blot (WB) and immunohistochemistry (IHC) assays.

Name	Company	Dilution for WB	Lot No.
EGF ab-3	Calbiochem (Darmstadt, Germany)	1:200	GF07L
EGFR	Upstate (Boulevard, CA, USA)	1:1000	06-847
phospho-EGFR (Tyr1086)	Upstate	1:1000	07-818
P-EGFR	Phospho-EGFR (Tyr1148)	1:1000	07-819
Phospho-Src (Tyr416)	Cell Signaling	1:1000	2101
Fak c20	Santa Cruz	1:200	sc-558
Ets2	Santa Cruz	1:200	sc-351x
CMet	Santa Cruz	1:200	sc-162
p-Met (Tyr 1234)	Santa Cruz	1:200	sc-101736
Hgf	Santa Cruz	1:200	sc-7949
Hgfa n-19	Santa Cruz	1:200	sc-1371
Itga1	Santa Cruz	1:200	Sc-271034

Table 2. *Cont.*

Name	Company	Dilution for WB	Lot No.
Itgb1	Santa Cruz	1:200	Sc-271034
Col1a1	Santa Cruz	1:200	sc-25974
Tcptp	Santa Cruz	1:200	Sc-21345
Cav-1 h-97	Santa Cruz	1:200	sc-7875
Pparg	Santa Cruz	1:200	Sc-7196
E-cadherin (H-108)	Santa Cruz	1:200	sc-7870
Ppara	Santa Cruz	1:2000	Sc-1985x
Igf1	Santa Cruz	1:200	Sc1422
Tgfa	Santa Cruz	1:200	Sc-1338
Tgfb1	Santa Cruz	1:200	Sc-146
Tgfbr2	Santa Cruz	1:200	Sc-220
Smad2-3	Santa Cruz	1:2000	Sc-6202x
Smad6-7	Santa Cruz	1:200	Sc-7004
Smad4	Santa Cruz	1:2000	sc-1909x
Fas	Santa Cruz	1:200	sc-74540
Tnfr1	Santa Cruz	1:200	sc-8436
p53 (FL-393)	Santa Cruz	1:333	sc-6243
Bag3	Abecam (Cambridge, UK)	1:2000	ab47107
Casp3	Santa Cruz	1:200	Sc-7148
Casp8	Santa Cruz	1:200	Sc-7890
Casp9	Santa Cruz	1:200	Sc-7885
P21 (c-19)	Santa Cruz	1:200	Sc-397
Cyclind1	Calbiochem	1:200	9940109
p-JNK (G-7)	Santa Cruz	1:200	sc-6254
Nek6	Abgent	1:100	AP8077a
h-ras	Santa Cruz	1:200	Sc-35
Raf1	Santa Cruz	1:200	Sc-133
Mek1	Abcam	1:200	Ab-32091-100
Erk1-2	Santa Cruz	1:200	Sc-135900
p-ERK (E-4)	Santa Cruz	1:200	sc-7383
Dusp6	Santa Cruz	1:200	Sc-137245
P38	Santa Cruz	1:200	Sc-7972
SOD1	Santa Cruz	1:200	Sc-8637
Stat5a	Santa Cruz	1:2000	Sc-1081x
P=stat5a	NEB (Ipswich, MA, USA)	1:200	9351s
Nfkb	Santa Cruz	1:100	sc-109
Ikkb	Santa Cruz	1:200	Sc-9130
c/ebpa	Santa Cruz	1:2000	Sc-61x
c/ebpb	Santa Cruz	1:2000	sc-150x

Table 2. *Cont.*

Name	Company	Dilution for WB	Lot No.
Hnf1a	Santa Cruz	1:200	Sc-6547x
Hnf3a	Santa Cruz	1:200	sc-6553
Hnf3b	Santa Cruz	1:100	sc-6554
Hnf4a	Santa Cruz	1:2000	Sc6556x
Hnf6	Santa Cruz	1:2000	Sc-6559x
Ahr	Biomed (Cambridge, UK)	1:200	SA-210
Cyp4a1	Santa Cruz	1:200	Sc-53247
Pcna	Santa Cruz	1:200	sc-7907
Cdk4	Santa Cruz	1:200	sc-260
b-catenin	Upstate	1:200	06-734
GAPDH (fl-355)	GAPDH (FL-335) (Santa Cruz, TX, USA)	1:200	sc-25778

Following extensive washing, the blot was developed using enhanced chemiluminescent detection (Perkin-Elmer, Juegesheim, Germany) and recorded using a Kodak IS 440CF imaging system (Kodak; Biostep GmbH, Jahnsdorf, Germany). GAPDH was used as a reference protein. All experiments were performed in triplicate.

2.8. Immunohistochemistry

After embedding in paraffin, fixed liver tissue was sectioned at a distance of 4–5 mm. The sections were de-paraffinized, rehydrated, and heated to boiling in 0.01 M citrate buffer (pH 6.0) in a microwave oven. After the portions boiled, they were cooked for a further 15 min on low heat. After that, the portions were blocked for 10 min at room temperature using 1.5% normal serum. The antisera c-Myc, c-Met, proliferative cell nuclear antigen (PCNA), and bromodeoxyuridine (BrdU) are included in Table 3 of the antibody list. The following 1:200 dilutions of antisera were used to incubate the liver sections for a whole night at room temperature. The DAKO Staining System was then used to visualize immunoreactivity (shown in brown) to the corresponding protein in accordance with the manufacturer's instructions. Normal rabbit or goat IgG was used in place of a primary antibody in the negative control sections for the anti-PCNA and anti-BrdU antisera. We used Mayer's hematoxylin as a counterstain for the sections. An Axiom vision light microscope and a Nikon DXM1200F digital camera were then employed to take pictures of the sections.

Table 3. The top tenfold alterations in genes show a substantial difference in gene expression (fold change is expressed in terms of normalized, untransformed data).

Gene Symbol	TCluster ID	Description	Fold Change	Differential Expression *p*-Value
Pcdh12	6864783	protocadherin12	1.41	3.54×10^{-2}
Snrk	6993055	SNF related kinase	1.51×10^{2}	5.01×10^{-2}
Ldb1	6873393	LIM domain binding 1	-1.41×10^{2}	6.87×10^{-2}
010Ertd641e	6774274	DNA segment Chr 10 ERATO	−1.71	7.50×10^{-2}
Prtl.rir	6962829	Interferon-inducible double-strand RNA activated protein kinase	−1.31	6.78×10^{-2}

Table 3. *Cont.*

Gene Symbol	TCluster ID	Description	Fold Change	Differential Expression *p*-Value
Adra1b	6787614	Adrenergic receptor alpha lb	2.91	6.17×10^{-2}
Fg11	6981914	Fibrinogen Fike protein 1	−2.41	7.35×10^{-2}
Serinc3	6892831	Serine inoorpora10 < 3	−1.81	7.77×10^{-2}
Npt1	6906895	Natriuretic peptide receptor 1	1.51	8.02×10^{-2}
Rbm3	7015454	RNA binding motif protein 3	−5.51	8.03×10^{-2}

2.9. Statistical Analysis

The study utilized a mixed model analysis of variance to compare six hybridizations of DEN treatments with six hybridizations of BHT at the age of 8.5 months. Exon array expression was normalized to the control non-transgenic background on the MouseExon10ST array. The analysis was conducted using XRAY software (version 3.2). Gene expression probes were normalized against historical data. FCs were considered significant at $p \leq 0.05$, and the Student's *t*-test was used for statistical analysis.

3. Results

3.1. Acceleration of Tumor Growth in ATT-Myc Transgenic Mice Treated with DEN

Figure 1A1,A2 presents the construction of an ATT-Myc mouse model of liver cancer and the expression of the c-Myc transgene as a PCR product in gel electrophoresis. The ratio of liver weight to body weight was significantly increased in 5.5–8.5-month-old ATT-Myc transgenic mice treated with DEN compared with transgenic mice treated with saline, BHT, or paracetamol. This increase in liver weight was due to rapid tumor growth, which is also shown in the overall image (see Figure 1B1,B2).

Notably, the liver parenchyma of non-transgenic mice showed no discernible alterations, with intact bile ducts, vasculature, and lobular architecture. Only a small percentage of transgenic animals exhibited uni- or multi-focal dysplastic liver nodules, affecting 10–80% of the liver parenchyma, with nodule sizes ranging from 1 to 10 mm. The hepatocytes in these foci displayed a nodular architecture, uni- to bi-cellular layers, and a maintained nuclear/cytoplasmic ratio. Pseudoglandular regions, cystic gaps within tumors, and multilayered trabecular architecture were observed in HCC (see Figure 1C1–C6). In some DEN-treated animals, metastasis of primary liver cancer to the lungs was observed. Additionally, in rodent bioassays, the primary target organs for DEN-induced carcinogenesis included the liver and lungs,

3.2. Gene Expression Differences Between Genotoxic and Non-Genotoxic Liver Carcinogens

Hierarchical clustering analysis (HCA) and principal component analysis (PCA) were performed to compare changes in gene expression in the livers of AAT-Myc transgenic mice treated with BHT and DEN at the age of 8.5 months with transgenic control mice given vehicles. The analysis was conducted on the FCs of 666 significantly regulated genes (SRGs). Compared to control transgenic mice, there were distinct differences, particularly at 8.5 months, in both HCA and PCA analyses. Additionally, the significance of these differences was greater when compared to non-transgenic control mice than when compared to transgenic mice (Figure 2).

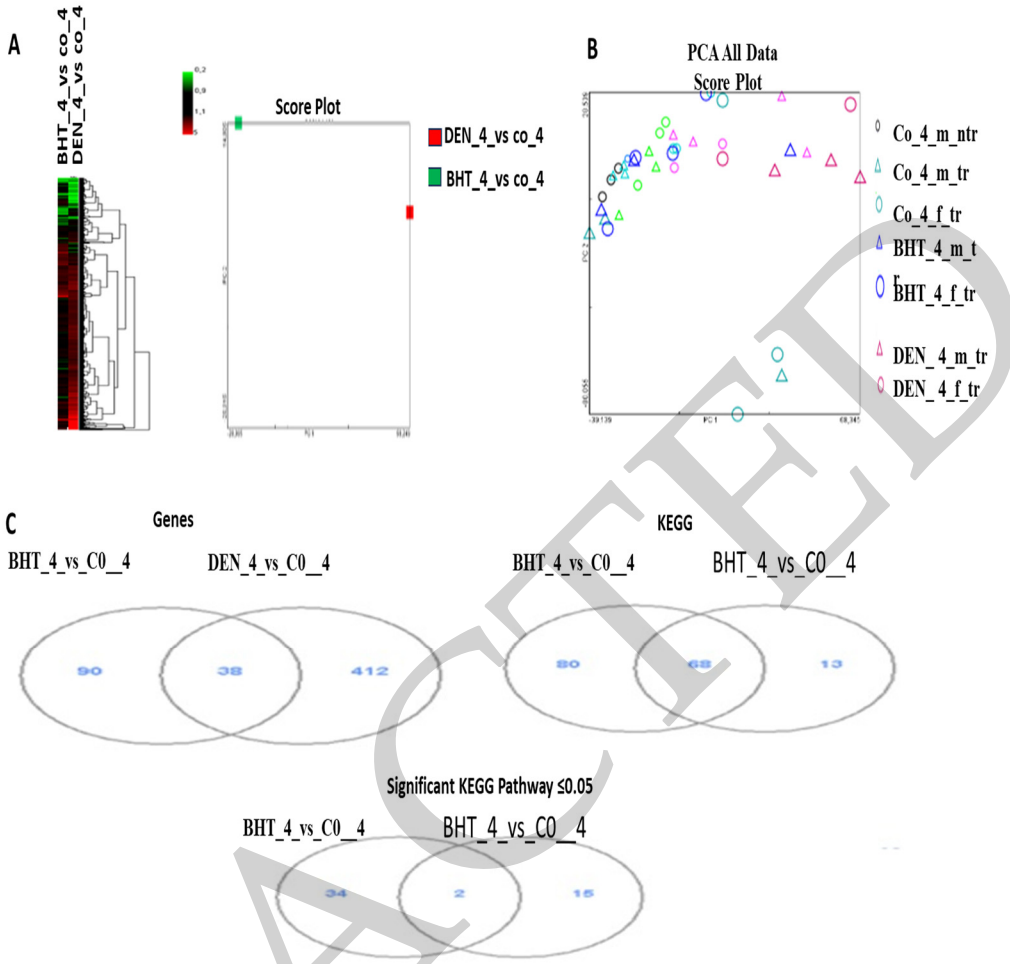

Figure 2. (**A**) shows HCA and PCA of gene expression changes in the livers of AAT-Myc transgenic mice induced by BHT and DEN at 8.5 months compared to transgenic control mice treated with a vehicle. FCs of 666 SRGs were analyzed. (**B**) presents the HCA and PCA of gene expression changes in the livers of AAT-Myc transgenic mice induced by BHT and DEN at 8.5 months compared to non-transgenic control mice treated with a vehicle, where FCs of 533 SRGs were analyzed. (**C**) illustrates PCA of the whole dataset of gene expression changes in the livers of AAT-Myc transgenic mice induced by BHT and DEN at 8.5 months compared to transgenic control mice treated with vehicles, with FCs of 666 SRGs included. The figure also depicts the volume differential (VD) analysis of genes significantly regulated in the liver of AAT-Myc transgenic mice treated with BHT and DEN versus transgenic control mice treated with vehicle (NaCl) at 8.5 months.

Once AAT-Myc transgenic mice were treated with BHT and DEN at the age of 8.5 months, their livers were analyzed using VD analysis to identify the genes that were significantly regulated. The results showed that 450 genes were significantly upregulated by DEN treatment, while only 128 genes were affected by BHT treatment. For both DEN and BHT, the most prevalent gene function pathway (KEGG) count was 148. For DEN, the significant KEGG pathway count was 36, while for BHT, it was 17 pathways. While BHT did not influence any of the genes linked to these pathways, DEN strongly regulated the cell cycle, DNA replication, p53 signaling pathway, mismatch repair, retinol metabolism, pyrimidine metabolism, and arachidonic acid metabolism. Furthermore, many more genes were regulated by DEN, and even though one or two genes were also regulated by BHT in several pathways, these pathways were not found to be significantly regulated.

Meanwhile, pathways largely controlled by BHT were mostly associated with drug detoxification and cellular metabolism, such as Cyp1a2 and Tpmt, which were downregulated in mice receiving DEN treatment. Additionally, most of the genes associated with

metabolism of xenobiotics by cytochrome P450 (KEGG), linoleic acid metabolism (KEGG), and arachidonic acid metabolism (KEGG) were downregulated in DEN-treated transgenic mice but remained unchanged in BHT-treated mice. Furthermore, the metabolism of ascorbate and aldarate (KEGG) was largely downregulated in DEN-treated mice but remained mostly intact with BHT therapy.

Notably, tumor growth in the DEN group was significantly correlated with an increase in transformed or carcinogenic hepatocyte proliferation, which requires increased glucose metabolism. This included upregulation of Glut-1 and subsequent upregulation of glycosaminoglycan degradation (KEGG), starch and sucrose metabolism (KEGG), pentose phosphate pathway (KEGG), fructose and mannose metabolism (KEGG), other glycan degradation (KEGG), glycosphingolipid biosynthesis ganglioside (KEGG), galactose metabolism (KEGG), and inositol phosphate metabolism (KEGG). Conversely, livers with advanced disease progression were unable to process lipids, as evidenced by the downregulation of fatty acid metabolism (KEGG), linoleic acid metabolism (KEGG), and arachidonic acid metabolism (KEGG).

There were 270,096 transcript clusters in total in the MouseExon10ST array. Upon applying the designated criteria, 8090 clusters containing between 4 and 200 probe sets were identified. These clusters were subsequently tested for alternative splicing and differential gene expression using the previously described statistical techniques. An overview of the expressed genes (transcript clusters) in each group among the tested clusters is given in the transcript clusters below.

Group	Number of transcript clusters with significant expression in the group	
DEN_4_mf	7501	92.7% of genes tested
bht_4_mf	7162	88.5% of genes tested

Using the same test, the following deferential comparison of gene expression summarizes frequencies of pairwise co-expression between the study groups.

	DEN	BHT
DEN	-	7 (0.609)
BHT	7162 (0.270)	-

The unmodified number is inclusive, while the figures in parentheses, if supplied, indicate exclusivity. For example, the DEN_4_mf group is significantly expressed above the background in 7501 genes, and is solely expressed in 609 genes without any other group exceeding the background. All co-expression patterns are summarized in the following table, which shows frequencies only. For example, the group DEN_4_mf+bht_4_mf is solely expressed by 6892 genes, and no other tissues exhibit expression above the background.

DEN_4_mf+bht_4_mf 6892
DEN_4_mf 609
bht_4_mf 270

3.2.1. Differential Gene Expression and Alternative Splicing

Six hundred and three genes showed statistically significant variations in gene expression across the groups, according to the statistical analysis described in the Section 2. Furthermore, 434 genes demonstrated substantial exon-group interaction, suggesting alternative splicing; of these, 71 genes showed significant variations in gene expression as well as interaction. In Table 3, the top tenfold alterations in genes showing a substantial difference in gene expression when comparing DEN to BHT treatment in transgenic mice

are listed. The FC is expressed in terms of the normalized, untransformed data. Table 4 presents the top 10 genes with significant differential alternative splicing.

Table 4. The top 10 genes with significant differential alternative splicing.

Gene Symbol	TCluster ID	Description	Exon-Tissue *p*-Value
Dst	6748525	Dystonin	1.06×10^{-20}
Abcc6	6967022	ATP-binding cassette subfamily C (CFTR)	1.38×10^{-20}
Slc17a4	6811714	Solute carrier family 17 (sodium phosphate)	1.49×10^{-15}
Ivns1abp	6754014	Influenza virus NS1A binding protein	4.71×10^{-15}
Agxt2l2	6780858	Alanine-glyoxylate aminotransferase 2-li	2.19×10^{-10}
Fn1	6759621	Fibronectin 1	2.66×10^{-10}
Stab2	6775762	Stabilin 2	7.40×10^{-10}
Slc7a2	6975658	Solute carrier family 7 (cationic amino)	9.87×10^{-9}
Lipc	6996667	Lipase hepatic	9.11×10^{-8}
Pard3	6979993	Par-3 (partitioning defective 3) homolog	1.28×10^{-7}

False Discovery Rate

To ascertain that the false discovery rate for the differential alternative splicing and gene expression assays in this study is annotation below 8×10^3, the step-down approach previously described was utilized.

3.2.2. Examining and Contrasting Differentially Expressed Genes and Exons with Established Gene Classifications

Existing gene classifications were compared to the 8090 genes that were tested for differential alternative splicing and gene expression, as detailed in the MouseExon10ST.info file. The objective was to identify any significant over-representation in the GOMolFn, GOProcess, GOCellLoc, or Pathway classes (Figure 3). Contingency table analysis was utilized to identify the groups in which genes exhibiting significant splicing or expression changes were over-represented. Under random conditions, the distribution of key genes in a group is hypergeometric.

3.2.3. Significant Representation Within the GOMolFn Categorization Group

As identified by the procedure outlined for evaluating differential splicing and gene expression, 219 groupings within the GOMolFn gene categorization showed a notable over-representation within the list of differently spliced or expressed genes. Table 5 below shows the top 30 groups. The columns represent the group name, the number of tested genes exhibiting significant differential splicing (along with the corresponding *p*-value of over-representation), and the count of genes displaying significant differential gene expression (along with the corresponding *p*-value of over-representation). Each row corresponds to a distinct group (Table 5).

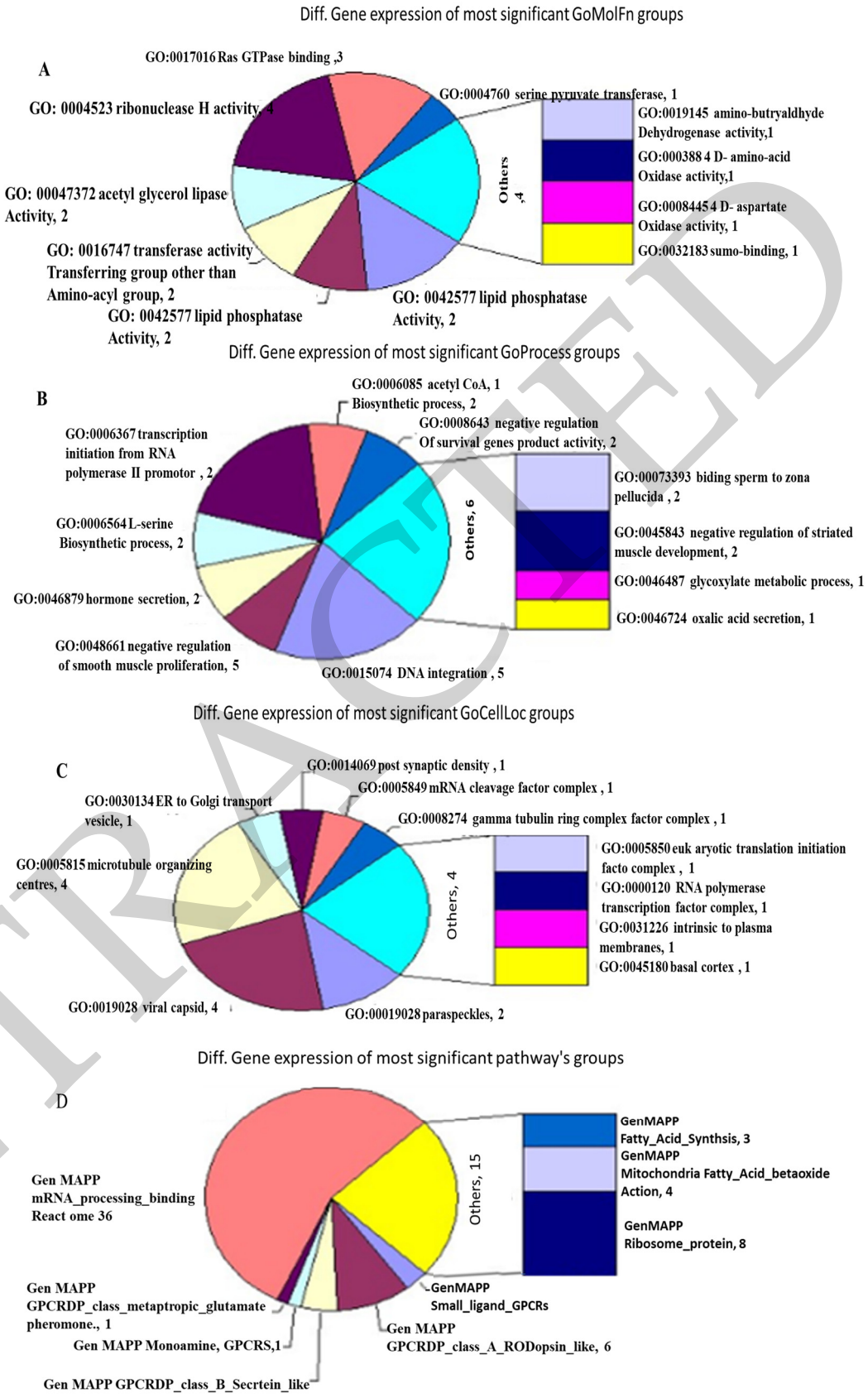

Figure 3. Group (**A**) represents most of the strongly varying gene expressions in the GOMolFn classification groups. Group (**B**) of the GOProcess classification exhibits the most significant gene expression. The GOCellLoc classification's group with significant gene expression is represented in (**C**), while group (**D**) shows significant gene expression within the Pathway classification group.

Table 5. The 30 most significantly differentially expressed genes in the GOMolFn classification group.

	Number GE	Number AS	Group Name
1	2 (7.90×10^{-3})	5 (0.00×10^{0})	GO:0016717 oxidoreductase activity
2	1 (9.08×10^{-2})	3 (3.18×10^{-10})	GO:0004768
3	0 (1.00×10^{0})	3 (3.18×10^{-10})	GO:0015020 glucuronosyltransferase activity
4	3 (5.20×10^{-10})	2 (1.22×10^{-6})	GO:0016298 lipase activity
5	1 (1.10×10^{-2})	2 (1.43×10^{-9})	GO:00311 Binding to phosphopantetheine
6	2 (3.13×10^{-7})	0 (1.00×10^{0})	GO:00425 lipid phosphatase activity
7	2 (3.13×10^{-7})	1 (2.54×10^{-3})	GO:0016747 acyltransferase activity
8	2 (3.13×10^{-7})	0 (1.00×10^{0})	G9O:0047372 acylglycerol lipase
9	1 (4.39×10^{-2})	2 (1.22×10^{-6})	Activity
10	1 (4.39×10^{-2})	2 (1.22×10^{-6})	GO:0003872 phosphofructokinase
11	1 (4.39×10^{-2})	2 (1.22×10^{-6})	GO:0005550 pheromone binding
12	0 (1.00×10^{0})	2 (1.22×10^{-6})	GO:0008559
13	12 (6.78×10^{-1})	24 (1.64×10^{-6})	GO:0008800 beta-lactamase activity
14	1 (2.46×10^{-1})	3 (5.35×10^{-6})	GO:0005506 iron ion binding
15	7 (4.53×10^{-1})	14 (8.90×10^{-6})	GO:0004467 long-chain fatty acid-CoA ligase activity
16	1 (2.13×10^{-4})	1 (1.33×10^{-5})	GO-0020037 heme binding
17	1 (2.13×10^{-4})	1 (1.33×10^{-5})	GO:0019103 pyrimidine nucleotide binding
18	1 (2.13×10^{-4})	1 (1.33×10^{-5})	GO:0004312 fatty-acid synthase activity
19	1 (2.13×10^{-4})	1 (1.33×10^{-5})	GO:0004313 [acy·l-cafrier-protein] S- acetyl coA
20	1 (2.13×10^{-4})	1 (1.33×10^{-5})	GO:0004314 acyl carrier proteinmalonyltransferase activity
21	1 (2.13×10^{-4})	1 (1.33×10^{-5})	GO:0004317 3-hydroxypalmitoyl-ACP dehydratase activity
22	1 (2.13×10^{-4})	1 (1.33×10^{-5})	GO:0004319 enoyl-(acyl-carrier protein)
23	1 (2.13×10^{-4})	1 (1.33×10^{-5})	GO:0004320 oleoyl-(acyl-carrier- protein)
24	1 (2.13×10^{-4})	1 (1.33×10^{-5})	GO:0010281 Acyl-ACP thioesterase
25	1 (2.13×10^{-4})	1 (1.33×10^{-5})	GO:0003865 3-oxo-5-alpha-steroid 4-dehydrogenase activity
26	1 (2.13×10^{-4})	1 (1.33×10^{-5})	GO:0004903 growth hormone receptor activity
27	1 (2.13×10^{-4})	1 (1.33×10^{-5})	GO:0017046 peptide hormone binding
28	1 (2.13×10^{-4})	1 (1.33×10^{-5})	GO:0050051 leukotriene-B4 20-monooxygenase activity
29	1 (2.13×10^{-4})	1 (1.33×10^{-5})	GO:0016213 linoleoyl-CoA desaturase activity
30	1 (2.13×10^{-4})	1 (1.33×10^{-5})	GO:0003987 acetate-CoA ligase activity

3.2.4. Significant Representation Within the GOProcess Classification Group

The top 30 most significant differential gene expressions in the GOProcess classification group, based on the previously reported method of evaluating differential splicing and gene expression, are reported. Two hundred and eighty-five groups in the GOProcess gene classification showed substantial over-representation within the set of differently spliced or expressed genes. Table 6 lists the top 30 groups, detailing the count of tested genes displaying significant differential splicing (along with the corresponding *p*-value of over-representation), the count of genes exhibiting significant differential gene expression (along with the corresponding *p*-value of over-representation), and the group name.

Table 6. The 30 most significantly expressed genes in the GOProcess group.

	Number GE	Number AS	Group Name
1	5 (1.51×10^{-7})	0 (1.00×10^{0})	GO:0015074 DNA integration
2	2 (3.13×10^{-7})	0 (1.00×10^{0})	GO:0048661 positive regulation of smooth
3	2 (3.13×10^{-7})	0 (1.00×10^{0})	GO:0046879 hormone secretion
4	2 (3.13×10^{-7})	0 (1.00×10^{0})	GO:0006564 L-serine biosynthetic process
5	1 (4.39×10^{-2})	2 (1.22×10^{-6})	GO:0006235 dTTP biosynthetic process
6	0 (1.00×10^{0})	2 (1.22×10^{-6})	GO:0030655 beta-lactam antibiotic
7	0 (1.00×10^{0})	2 (1.22×10^{-6})	GO:0046677 response to antibiotic
8	0 (1.00×10^{0})	2 (1.22×10^{-6})	GO:0006884 regulation of cell volume
9	1 (2.46×10^{-1})	3 (5.35×10^{-6})	GO:0042060 wound healing
10	0 (1.00×10^{0})	3 (5.35×10^{-6})	GO:0006559 L-phenylalanine catabolic process
11	7 (4.64×10^{-4})	7 (6.27×10^{-6})	GO:0006633 fatty acid biosynthetic process
12	1 (2.13×10^{-4})	1 (1.33×10^{-5})	GO:0042276 error-prone translation synthesis
13	1 (2.13×10^{-4})	1 (1.33×10^{-5})	GO:0016050 vesicle organization Biological Process
14	1 (2.13×10^{-4})	1 (1.33×10^{-5})	GO:0035249 synaptic transmission, glutamatergic
15	1 (2.13×10^{-4})	1 (1.33×10^{-5})	GO:0009223 pyrimidine deoxyribonucleotide
16	1 (2.13×10^{-4})	1 (1.33×10^{-5})	GO:0009264 deoxyribonucleotide catabolic
17	1 (2.13×10^{-4})	1 (1.33×10^{-5})	GO:0006702 androgen biosynthetic process
18	1 (2.13×10^{-4})	1 (1.33×10^{-5})	GO:0006636 fatty acid desaturation
19	1 (2.13×10^{-4})	1 (1.33×10^{-5})	GO:0009124 nucleoside monophosphate metabolic process
20	1 (2.13×10^{-4})	1 (1.33×10^{-5})	GO:0009133 nucleoside diphosphate biosynthetic process
21	1 (2.13×10^{-4})	1 (1.33×10^{-5})	GO:0006021 inositol biosynthetic process
22	1 (2.13×10^{-4})	1 (1.33×10^{-5})	GO:0050983 spermidine catabolic process
23	0 (1.00×10^{0})	1 (1.33×10^{-5})	GO:0031110 regulation of microtubule polymerization
24	0 (1.00×10^{0})	1 (1.33×10^{-5})	GO:0045104 intermediate filament cytoskeleton organization
25	0 (1.00×10^{0})	1 (1.33×10^{-5})	GO:0019585 glucuronate metabolic process
26	0 (1.00×10^{0})	1 (1.33×10^{-5})	GO:0001811 negative regulation of type I
27	0 (1.00×10^{0})	1 (1.33×10^{-5})	GO:0002862 negative regulation of inflammatory response
28	0 (1.00×10^{0})	1 (1.33×10^{-5})	GO:0002839 positive regulation of immune
29	0 (1.00×10^{0})	1 (1.33×10^{-5})	GO:0032816 positive regulation of natural killer cell activation.
30	0 (1.00×10^{0})	1 (1.33×10^{-5})	Group Name

3.2.5. Significant Representation Within the GOCellLoc Group

As identified by the previously outlined method of evaluating differential splicing and gene expression, 44 groups demonstrated considerable over-representation within the set of differentially spliced or expressed genes in the significant representation category of the GOCellLoc classification. Table 7 lists the top 30 groups, with each row corresponding to a different group. The columns indicate the group name, the number of tested genes exhibiting significant differential splicing (accompanied by the corresponding *p*-value of over-representation), and the count of genes displaying significant differential gene expression.

Table 7. The 30 significantly expressed genes in the GOCellLoc classification.

	Number GE	Number AS	Group Name
1	2 (3.13×10^{-7})	0 (1.00×10^{0})	GO:0042382 paraspeckles
2	1 (4.39×10^{-2})	2 (1.22×10^{-6})	GO:0005945 6-phosphofructokinase complex
3	2 (1.67×10^{-2})	3 (5.35×10^{-6})	GO:0046581 intercellular canaliculus
4	0 (1.00×10^{0})	3 (5.35×10^{-6})	GO:0017053 transcriptional repressor complex
5	1 (2.13×10^{-4})	1 (1.33×10^{-5})	GO:0014069 postsynaptic density
6	0 (1.00×10^{0})	1 (1.33×10^{-5})	GO:0005674 transcription factor TFIIF complex
7	0 (1.00×10^{0})	1 (1.33×10^{-5})	GO:0019815 B cell receptor complex
8	0 (1.00×10^{0})	1 (1.33×10^{-5})	GO:0042571 immunoglobulin complex
9	0 (1.00×10^{0})	1 (1.33×10^{-5})	GO:0009346 citrate lyase complex
10	0 (1.00×10^{0})	1 (1.33×10^{-5})	GO:0031074 nucleocytoplasmic shuttling complex
11	0 (1.00×10^{0})	1 (1.33×10^{-5})	GO:0001917 photoreceptor inner segment
12	0 (1.00×10^{0})	1 (1.33×10^{-5})	GO:0008352 Katanin complex
13	0 (1.00×10^{0})	1 (1.33×10^{-5})	GO:0000137 Golgi cis cisterna
14	4 (1.31×10^{-4})	1 (2.92×10^{-1})	GO:0019028 viral capsid. Cellular Component
15	4 (1.31×10^{-4})	0 (1.00×10^{0})	GO:0005815 microtubule organizing center
16	1 (2.13×10^{-4})	0 (1.00×10^{0})	GO:0030134 ER to Golgi transport vesicle
17	1 (2.13×10^{-4})	0 (1.00×10^{0})	GO:0005849 mRNA cleavage factor complex
18	1 (2.13×10^{-4})	0 (1.00×10^{0})	GO:0008274 gamma-tubulin ring complex
19	1 (2.13×10^{-4})	0 (1.00×10^{0})	GO:0005850 eukaryotic translation initiation factor 2 complex
20	1 (2.13×10^{-4})	0 (1.00×10^{0})	GO:0000120 RNA polymerase I transcription regulator
21	1 (2.13×10^{-4})	0 (1.00×10^{0})	GO:0031226 intrinsic to plasma membrane
22	1 (2.13×10^{-4})	0 (1.00×10^{0})	GO:0045180 basal cortex
23	1 (2.13×10^{-4})	0 (1.00×10^{0})	GO:0019185 snRNA-activating protein comp
24	1 (2.13×10^{-4})	0 (1.00×10^{0})	GO:0030530 heterogeneous nuclear ribonucleoprotein
25	1 (2.13×10^{-4})	0 (1.00×10^{0})	GO:0030014 CCR4-NOT complex
26	1 (2.13×10^{-4})	0 (1.00×10^{0})	GO:0005672 transcription factor TFllA complex
27	1 (2.13×10^{-4})	0 (1.00×10^{0})	GO:0000506 glycosylphosphatidylinositol-N-acetylglucosaminyl-transferase (GPI-GnT) complex
28	2 (5.98×10^{-4})	1 (4.0×10^{-2})	GO:0043197 dendritic spine
29	2 (5.98×10^{-4})	0 (1.00×10^{0})	GO:0019005 SCF ubiquitin ligase complex
30	3 (1.56×10^{-3})	1 (2.22×10^{-1})	GO:0005669 transcription factor TFllD complex

3.2.6. Significant Representation Within the Pathway Classification Group

Using the previously published method of evaluating differential splicing and gene expression, nine groups within the Pathway gene classification group showed a substantial over-representation among the set of genes that were either expressed or differentially spliced. Table 8 lists the top nine groups, with each row representing a different group.

Table 8. The nine most significantly expressed genes in the Pathway classification group.

	Number GE	Number AS	Group Name
1	2 (3.13×10^{-7})	0 (1.00×10^{0})	GenMAPP Small_ligand_GPCRs
2	6 (6.20×10^{-6})	0 (1.00×10^{0})	GenMAPP GPCRDB_Class_A_Rhodopsin-like
3	3 (1.81×10^{-4})	1 (1.47×10^{-1})	GenMAPP GPCRDB_Class_B_Secretin-like
4	1 (2.13×10^{-4})	0 (1.00×10^{0})	GenMAPP Monoamine_GPCRs
5	1 (2.13×10^{-4})	0 (1.00×10^{0})	GenMAPP GPCRDB_Class_C_Metabotropic_glutamate receptors
6	3 (3.32×10^{-3})	3 (2.73×10^{-4})	GenMAPP Fatty_Acid_Synthesis
7	36 (1.56×10^{-3})	22 (6.93×10^{-2})	GenMAPP mRNA_processing_binding_Reactom
8	4 (3.77×10^{-3})	2 (1.03×10^{-1})	GenMAPP Mitochondrial_fatty_acid_betaoxi
9	8 (9.02×10^{-3})	6 (1.63×10^{-2})	GenMAPP Ribosomal_Proteins

3.3. Confirmation of Gene Expression by Rt-PCR

Microarray gene expression data revealed an increase in the levels of rpl23, rfc4, mmp12, and bzwz compared to the non-transgenic control. Conversely, c9 exhibited a reduction, and there were no observed changes in dynll1, slc10a, gas6, and the housekeeping gene b-actin (Figure 4).

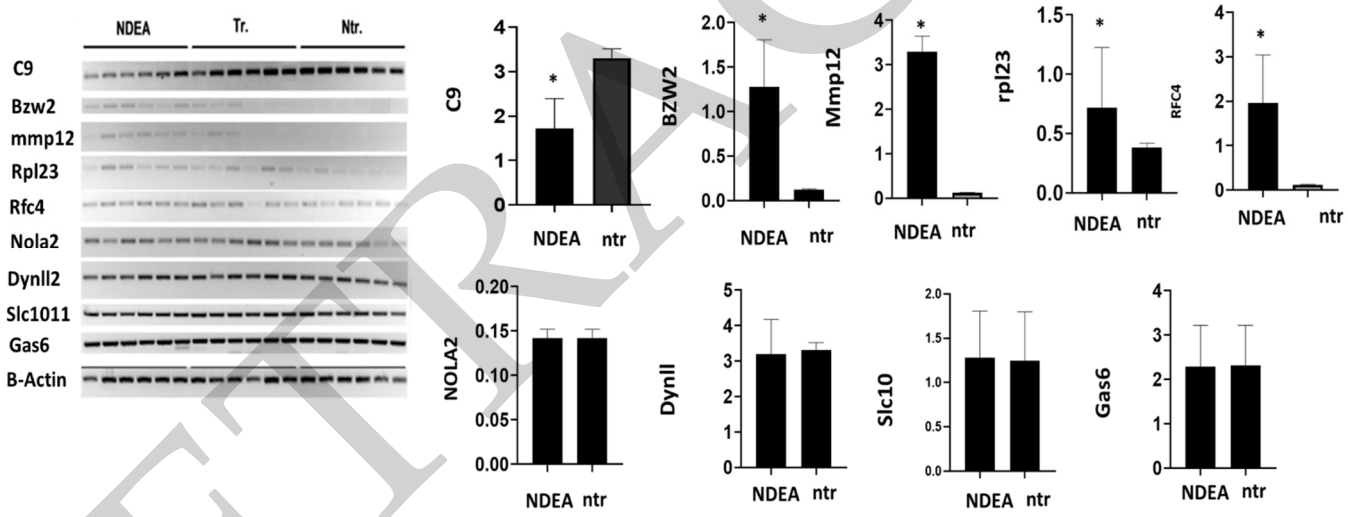

Figure 4. RT-PCR products were analyzed using gel electrophoresis and visualized using Kodak Image Station 440CF under UV light to validate exon array expression. All samples were normalized to β-actin levels. The densometrical scan of the gene expression analysis showed elevated levels of RPL23, RFC4, MMP12, and BZWZ after treatment with DEN in comparison to the non-transgenic control. In contrast, C9 displayed a decrease, while no significant variations were detected in DYNL1, SLC10A, GAS6, or the housekeeping gene β-actin. * $p < 0.05$.

3.4. Protein Expression Explored by Western Blotting of Treated Groups

Remarkably, DEN therapy resulted in a greater loss of HGF/c-Met signaling, which may have contributed to the tumor's rapid growth. Specifically, only ATT-Myc HCC mice that were untreated at the 12-month mark exhibited a decrease in c-Met. Meanwhile, BHT did not accelerate tumor growth at the experimental dose and instead preserved c-Met expression, similar to the control group. Notably, compared to the non-transgenic control group, c-Myc expression was consistently elevated by a factor of 12 in all treatment groups at both gene and protein levels. This suggests that the loss of c-Met/HGF signaling, accom-

panied by a loss of antioxidants such as superoxide dismutase (SOD1) and NRF2, and its down regulation led to enhancement of liver tumor growth in the c-myc model of liver cancer by promoting a more favorable environment for cancerous growth. This enhancement was observed four months after DEN treatment. Additional factors contributing to unchecked tumor proliferation include DNA damage, increased ROS production, loss of tumor suppressors such as p53, and compromised tissue repair systems (Figure 5A–D).

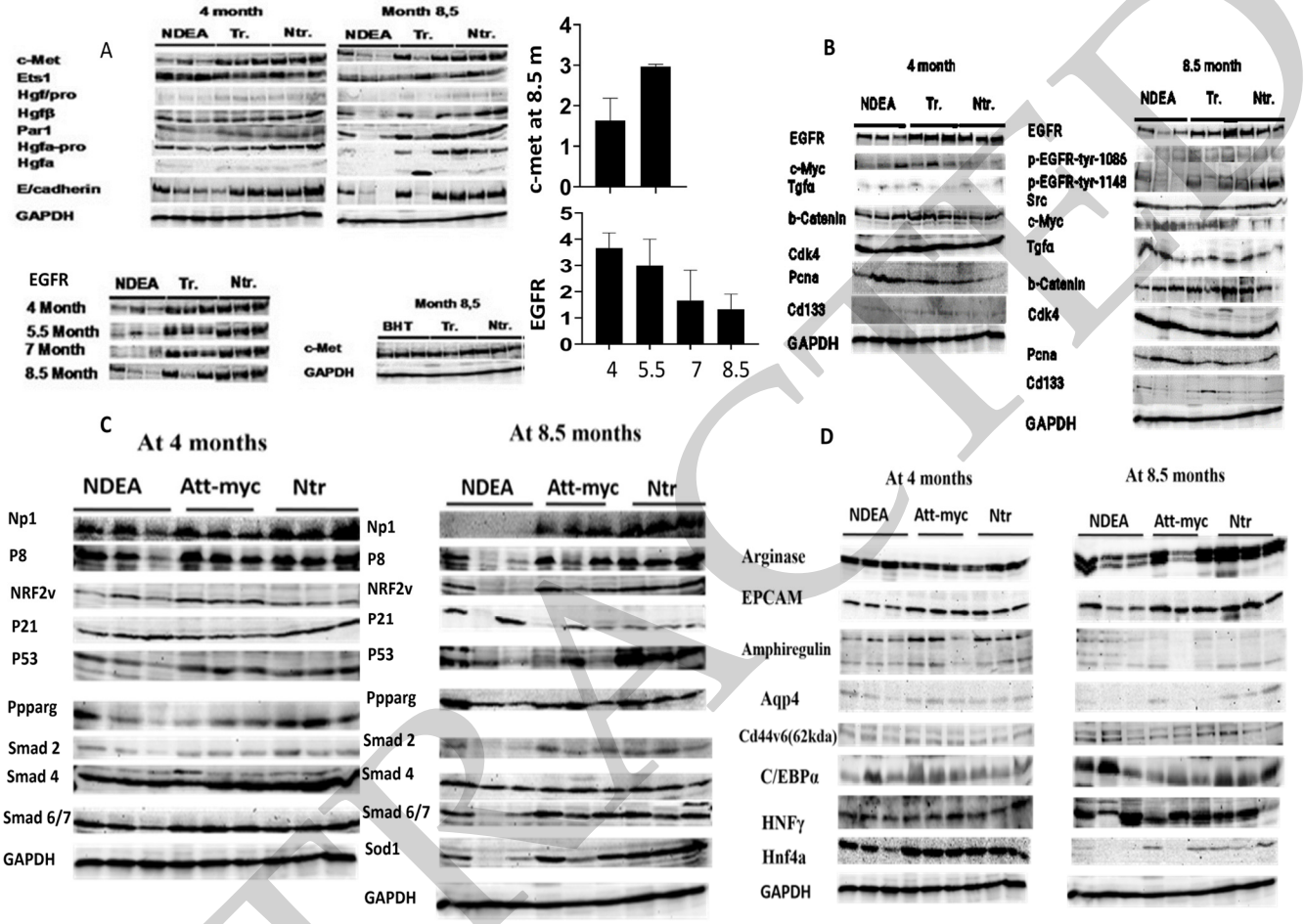

Figure 5. (**A**) This shows the loss of c-Met and its transcriptional factor ETS1 in liver tumors after DEN treatment at 8.5 months. (**B**) Loss of c-Met is time-dependent in liver tumors induced by DEN at different time points, while BHT maintains c-Met expression. additionally, Liver protein extracts from DEN-treated transgenic mice showing increased expressions of c-Myc, TGFα, PCNA, and CDK4 contributing to accelerated tumor growth. (**C**) DEN treatment enhances the loss of antioxidants, such as SOD1, NRF2, Neuropilin-1 (NP-1), and PPARγ, compared to control non-transgenic animals at 8.5 months. (**D**) DEN treatment reduces enriched transcriptional factors, such as HNF4α and HNFγ, while increasing the expression of C/EBPα and CD44 compared to control transgenic and non-transgenic mice.

3.5. Immunohistochemistry of DEN-Treated ATT-Myc Transgenic Mice

Remarkably, the DEN group exhibited an elevated proliferation rate of carcinogenic cells, as indicated by an increase in cells positive for PCNA or BrdU. Immunohistochemical detection of liver tumor tissue revealed an increase in c-Myc expression and a reduction in c-Met expression in DEN-treated mice compared to control transgenic mice (Figure 6).

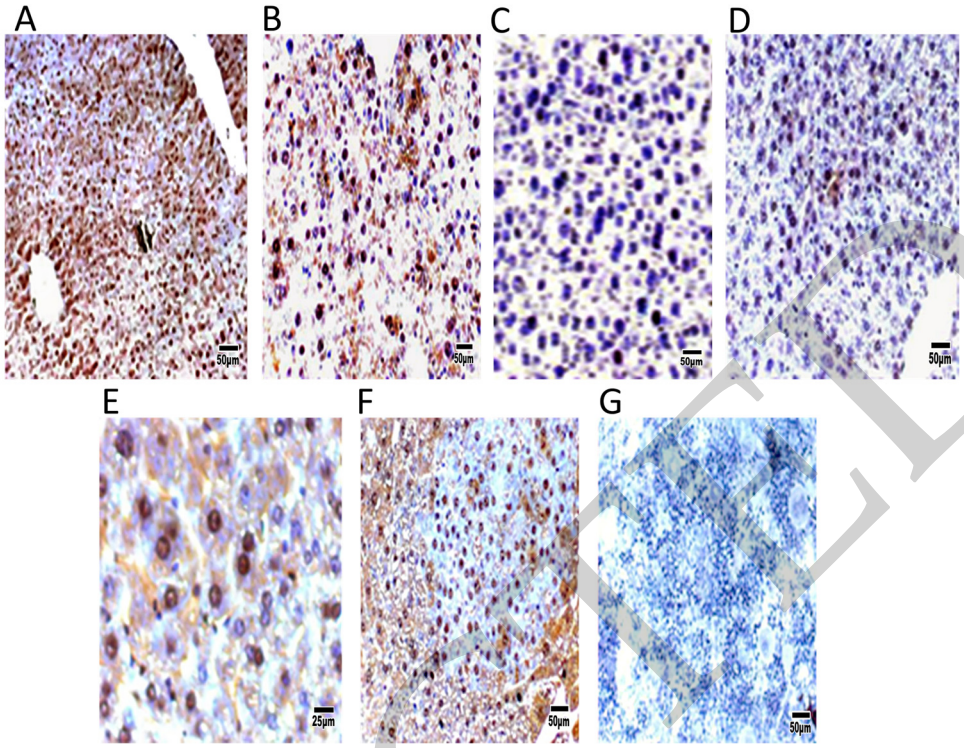

Figure 6. Immunohistochemistry staining demonstrated increased c-Myc expression in transgenic mice (**A**), while the distribution of c-Met expression was uneven (**B**). The unstained control group provided a reference for comparison (**C**). Increased PCNA expression was noted in DEN-treated mice (**D**) compared to the BHT-treated group (**E**), along with increased BrdU in the BHT-treated group (**F**). (**G**) shows control unstained sections.

4. Discussion

We previously examined the genotoxic carcinogen DEN and the non-genotoxic compound BHT as a proof of concept and found that DEN enhanced liver tumor growth in c-Myc as early as four months after the end of treatment [3]. According to the current study, the liver mass increased as soon as the DEN treatment ended (Figure 2), while the c-Myc transgenic model genetically caused hepatocellular cancer in mice at 12 months of age [2].

The fact that DEN therapy failed to cause tumors in other genetic models, such as rasH2 and p53 defective mice, in six months is extremely significant [4,5]. According to histopathology, transgenic mice given BHT only showed dysplastic nodules until the end of their lives or at 8.5 months. All things considered, the c-Myc transgenic mouse model responded to a genotoxic carcinogen and could distinguish between safe and dangerous substances, as seen by the HCC that appeared at 5.5 months of age. This result is in line with findings from c-Met knock-out mice treated with DEN, where tumor growth was also increased following DEN treatment [6]. Thus, shortening the time of cancer bioassays in the ATT-Myc model may accelerate the carcinogenicity testing of chemicals compared to old classic methods.

At 8.5 months, we used mixed model analysis of variance to examine 16 additional hybridizations on the MouseExon10ST array in order to confirm the selection of the most important genes that were elevated in the liver tumors that formed after DEN treatment. There were 434 genes with significant exon-group interactions (a marker of alternative splicing) and about 603 genes with significant gene expression changes across the groups; 71 genes had both gene and potential splicing differences ($p < 0.01$). The SNRK (SNF-Related Kinase) gene belongs to the family of serine/threonine kinases known as sucrose non-fermenting–related kinases and is one of the important genes expressed at 8.5 months [7].

Previous array data demonstrated that SNRK overexpression increased the levels of genes involved in cell proliferation. Moreover, SNRK increased CacyBP mRNA and protein and decreased β-catenin protein in HCT116 and RKO colon cancer cells [8]. After 8.5 months, DEN treatment led to the expression of Alpha1b. adrenergic receptor gene (Adra1b). Similarly, Alpha1 and α2c adrenergic receptor genes were over-expressed in basal-like breast tumors with poor prognosis [9].

In the present array data, Fgl1 was downregulated 8.5 months after DEN treatment. This is in line with the study by Nayeb-Hashemi et al. [10], who found that Fgl1 expression is decreased in HCC and that its loss correlates with a poorly differentiated phenotype.

In the c-Myc transgenic model of liver cancer, the emergence of large liver tumors and the loss of c-Met signaling were noted at 12 months of age [2]. In the current investigation, we first showed that at different times throughout the mice's lives, the genotoxic DEN increased the loss of c-Met and the aggressiveness of liver cancer growth. While the BHT-treated group and the transgenic vehicle-treated group did not exhibit any liver tumor growth that was confirmed by histological analysis, they preserved the expression of c-Met, except for one of the three transgenic mice at 8.5 months. Similarly, in c-Met knockout animals given DEN treatment, c-Met deletion increased liver tumor growth [6]. Notably, persistent BHT maintained c-Met expression and reversed the detrimental consequences of c-Met depletion. Therapy with N-acetyl-L-cysteine, an antioxidant, and decreasing DEN initiated hepatocarcinogenesis in Cre-Ctrl mice [6].

Furthermore, after 12 months, the liver weight of the c-Myc transgenic mice increased significantly, reaching 10% of the body weight by 16 months. This was indicative of the development of enormous liver tumors. Conversely, the liver weight of double transgenic c-Myc/HGF mice that were older than a year did not show any variation from their younger counterparts [2]. Similarly, the expression of the shortened c-Met transgene produced immortalized and non-transformed hepatocyte cell lines and induced tolerance to apoptotic stimuli in vivo [11]. The present investigation revealed the downregulation of antioxidant pathways, such as SOD1 and NRF2, along with c-Met expression, particularly at the age of 8.5 months. Thus, the expression of HGF/c-Met has been identified as a crucial regulator of cellular redox homeostasis and oxidative stress [12]. Unstimulated Met-knockout cells experienced oxidative stress, as evidenced by elevated ROS production. This was associated with increased Nicotinamide adenine dinucleotide phosphate (NADPH) and Rac1 activities, which were suppressed by known NADPH oxidase inhibitors. Furthermore, oxidative stress correlated with enhanced lipid peroxidation and reduced glutathione (GSH) levels. Administration of N-acetylcysteine, an antioxidant and GSH precursor, notably reduced agonistic anti-Fas (Jo2)-induced cell death [13]. Additionally, Takami et al. [6] reported that the detrimental effects of c-Met deficiency were alleviated by long-term oral administration of the antioxidant N-acetyl-l-cysteine. This treatment inhibited EGFR activation and reduced N-nitrosodiethylamine-induced hepatocarcinogenesis to levels observed in Cre-Ctrl mice. Similarly, BHT, considered an antioxidant, maintained c-Met expression and did not promote liver cancer in the ATT-Myc liver of the transgenic model.

Furthermore, the genetic deletion of c-Met in hepatocytes disrupts redox homeostasis [13]. Moreover, the development of liver-specific c-Met–knockout mice has demonstrated the significance of HGF/c-Met signaling in the control of cellular redox state by regulating the expression of antioxidant proteins and a parallel inhibition of pro-oxidant systems [14]. In the current study, DEN-treated mice reduced the NP-1 protein in liver tumor tissue in comparison to transgenic and non-transgenic control mice at the age of 8.5 months. In this regard, NP-1 controls endothelial homeostasis by regulating mitochondrial function and iron-based oxidative stress [15].

Notably, DEN, as a genotoxic carcinogen, enhanced ROS production in the liver tumor microenvironment [16] and the loss of an antioxidant such as SOD1 [6]. In the current study, DEN treatment enhanced the loss of enriched transcriptional factors, such as HNF4a1 and HNFγ [2], due to extensive DNA damage and expression of C/EBPα. In this regard, there was a correlation between the expression of enriched transcriptional factors in hepatocytes and the cyto-met expression [16] in cell lines and transgenic models [11]. Moreover, in the current study, the c-Myc gene expression increased 12-fold after DEN treatment, and c-Myc protein expression was monitored by IHC. In this regard, previous reports showed that the loss of p53-mediated genomic surveillance and over-expression of c-Myc result in the suppression of DNA repair and enhancement of the mutation rate in cancer cells [18], and once the tumors become established, c-Myc is a key gene player in alternative macrophage activation and pro-tumorigenic gene expression [2]. While DEN enhanced the liver tumors in other transgenic models after six months of treatment [4,5], the expression of c-Myc and c-Met in a double transgenic mouse model (WHV/c-Myc transgenic mice) induced a dramatic increase in Myc-induced tumorigenesis in animals as young as 3–4-months old [1].

Intriguingly, the mechanism of the loss of c-Met signaling in the current study was due to the loss of its transcriptional factor (ets1), as the expression of c-Myc suppressed the expression of ets1 and consequently enhanced the loss of c-Met [17]. There was also extensive ROS production in the liver microenvironment due to the high expression of c-Myc. [18]. Notably, treatment with an antioxidant such as N-acetyl-l-cysteine in previous studies maintained c-Met expression and protected against DEN treatment [6]. Likewise, BHT treatment maintained hepatocytes in the dysplastic stage and prevented their conversion into liver tumors. Moreover, the use of a herbal extract, with quercetin as the active component, targeted c-Myc directly via reduction of ROS production [19,20] or release of exosomes from tumor cells under hypoxic conditions [21].

The ETS family TF—ETS1—was recognized as a key regulator of the intrahepatic cholangiocarcinoma lineage, which Myc was found to suppress during HCC progression. Notably, shRNA-mediated knockdown of FOXA1 and FOXA2, along with sustained ETS1 expression, completely shifted HCC to intrahepatic cholangiocarcinoma development in primary liver cancer mouse models [22].

Conclusions: In the ATT-Myc liver cancer model, the persistent upregulation of c-Myc at both gene and protein levels inhibits the ETS1 transcription factor, further aggravating the decline of c-Met signaling, SOD1, and NRF2. This increased ROS production and promoted rapid liver tumor growth. The present study reinforces the potential of a monoclonal antibody targeting c-Myc as a therapeutic strategy for liver cancer, underscoring its significance in future clinical research. Moreover, it encourages researchers to finalize the validation of the ATT-Myc model as a liver tumor model alongside the Rash2 transgenic model.

The limitation of the current study is the cost of validation, as developing alternative short-term toxicity research is still expensive. However, once the model is validated, testing chemicals will become cheaper and take less time.

Author Contributions: M.E., A.J.A. and M.G.E. designed the study, conducted the experiments, analyzed the data, and revised the manuscript. M.E. prepared the result figures. All authors have read and agreed to the published version of the manuscript.

Funding: This work was supported by the Deanship of Scientific Research, Vice Presidency for Graduate Studies and Scientific Research, King Faisal University, Saudi Arabia (Project No. GRANT-KFU250379).

Institutional Review Board Statement: The study was conducted in accordance with the Declaration of Helsinki and approved by the Institutional Review Board (the Ethical Committee of Hannover, Ger-

many, AZ:.33.9-42502-04-08/1619 march, 2009 & the ethical committee of the King Faisal University (KFU-25-ETHIC53114, January 2025).

Informed Consent Statement: Not applicable.

Data Availability Statement: Data are provided within the manuscript.

Acknowledgments: We thank Roman Halter, a postdoctoral researcher who helped during the experimental stage at the Fraunhofer Institute of Toxicology and Experimental Medicine (Hanover, Germany). In addition, we are grateful to Reinhard Spanel, who supported us in the pathological examination of the ATT-Myc liver tumor. Moreover, we thank Tatiana Miere, a postdoctoral researcher who supported us with gene expression on array tracking of liver tumors.

Conflicts of Interest: The authors have no conflict of interest.

Abbreviations

ATT-myc	Alpha-1-antitrypsin-c-myc transgenic model
Abl	Abelson murine leukemia oncogene 1
Bag3	family molecular chaperone regulator 3
C/ebpa,b	CCAAT/enhancer-binding protein alpha, beta
C-Abl	Tyrosine kinase ABL1
Casp3	Caspase 3
Casp8	Caspase 8
Casp9	caspase 9
Cav-1	Caveolin-1
CMet	Hepatocyte growth factor receptor
Col1a1	Collagen 1a1
EGF	Epidermal growth factor
EGFR	Epidermal growth factor receptor
ERKs	Extracellular-signal-regulated kinases
FAK	Focal Adhesion Kinase
FAS (CD95)	FAS-legand apoptosis pathway
HGF	Hepatocyte growth factor
HGFA	Hepatocyte growth factor activator
HNF	Hepatocyte nuclear factor
HSC	hepatocyte stellate cells
IGF1	Insulin-like growth factor 1
Ikkb	inhibitor of nuclear factor kappa-B kinase subunit beta
INTGα1	Integrin alpha1
INTGβ1	Integrin Beta 1
Jnk	C-Jun N-terminal kinases
Nek 6	NIMA (never in mitosis)-related kinase 6
NF-kb	nuclear factor kappa-light-chain-enhancer of activated B
Ntr	non-transgenic or wild
PAI-1	Plasminogen activator inhibitor-1
Pparα	Peroxisome proliferator-activated receptor alpha
Pparγ	Peroxisome proliferator-activated receptor gamma
SOD1	Superoxide dismutase
Src	Rous sarcoma oncogene
TF	Transcription factor
Tr	transgenic
ntr	Non-transgenic
TGFa	Transforming growth factor alpha
TGFb1	Transforming growth factor beta 1
TGFbr2	Transforming growth factor beta receptor 2

TNF-r1	tumor necrosis superfamily receptor 1
BHT_4_m_tr	BHT-treated mice for fourth sacrifice or 8.5 months, male, transgenic
BHT_4_f_tr	BHT-treated mice for fourth sacrifice or 8.5 months, female, transgenic
DEN_4_m_tr	DEN-treated mice for fourth sacrifice or 8.5 months, male, transgenic
DEN_4_f_tr	DEN-treated mice for fourth sacrifice or 8.5 months, female, transgenic
Co_4_m_ntr	Comparison with male non-transgenic mice as a background
Co_4_m_tr	Comparison with male transgenic mice as a background
Co_4_f_tr	Comparison with female transgenic mice as a background

References

1. Dalemans, W.; Perraud, F.; Le Meur, M.; Gerlinger, P.; Courthey, M.; Pavirani, A. Heterologous protein expression by transimmortalized differentiated liver cell lines derived from transgenic mice (hepatomas/α1 antitrypsin/ONC mouse). *Biologicals* **1990**, *18*, 191–198. [CrossRef] [PubMed]
2. Santoni-Rugiu, E.; Preisegger, K.H.; Kiss, A.; Audolfsson, T.; Shiota, G.; Schmidt, E.V.; Thorgeirsson, S.S. Inhibition of neoplastic development in the liver by hepatocyte growth factor in a transgenic mouse model. *Proc. Natl. Acad. Sci. USA* **1996**, *93*, 9577–9582. [CrossRef]
3. Hueper, K.; Elalfy, M.; Laenger, F.; Halter, R.; Rodt, T.; Galanski, M.; Borlak, J. PET/CT imaging of c-Myc Transgenic mice identifies the genotoxic N-nitroso-diethylamine as carcinogen in a short-term cancer bioassay. *PLoS ONE* **2012**, *7*, e30432. [CrossRef] [PubMed]
4. Finnberg, N.; Stenius, U.; Högberg, J. Heterozygous p53-deficient (+/−) mice develop fewer p53-negative preneoplastic focal liver lesions in response to treatment with diethylnitrosamine than do wild-type (+/+) mice. *Cancer Lett.* **2004**, *207*, 149–155. [CrossRef]
5. Usui, T.; Mutai, M.; Hisada, S.; Takoaka, M.; Soper, K.A.; Mccullough, B.; Alden, C. CB6F1-rasH2 mouse: Overview of available data. *Toxicol. Pathol.* **2001**, *29*, 90–108. [CrossRef] [PubMed]
6. Takami, T.; Kaposi-Novak, P.; Uchida, K.; Gomez-Quiroz, L.E.; Conner, E.A.; Factor, V.M.; Thorgeirsson, S.S. Loss of hepatocyte growth factor/c-Met signaling pathway accelerates early stages of *N*-nitrosodiethylamine–induced hepatocarcinogenesis. *Cancer Res.* **2007**, *67*, 9844–9851. [CrossRef] [PubMed]
7. Kertesz, N.; Samson, J.; Debacker, C.; Wu, H.; Labastie, M.-C. Cloning and characterization of human and mouse SNRK sucrose non-fermenting protein (SNF-1)-related kinases. *Gene* **2002**, *294*, 13–24. [CrossRef]
8. Rines, A.K.; Burke, M.A.; Fernandez, R.P.; Volpert, O.V.; Ardehali, H. Snf1-related kinase inhibits colon cancer cell proliferation through calcyclin-binding protein-dependent reduction of β-catenin. *FASEB J.* **2012**, *26*, 4685. [CrossRef]
9. Powe, D.G.; Voss, M.J.; Habashy, H.O.; Zänker, K.S.; Green, A.R.; Ellis, I.O.; Entschladen, F. Alpha- and beta-adrenergic receptor (AR) protein expression is associated with poor clinical outcome in breast cancer: An immunohistochemical study. *Breast Cancer Res. Treat.* **2011**, *130*, 457–463. [CrossRef]
10. Nayeb-Hashemi, H.; Desai, A.; Demchev, V.; Bronson, R.T.; Hornick, J.L.; Cohen, D.E.; Ukomadu, C. Targeted disruption of fibrinogen like protein-1 accelerates hepatocellular carcinoma development. *Biochem. Biophys. Res. Commun.* **2015**, *465*, 167–173. [CrossRef]
11. Amicone, L.; Spagnoli, F.M.; Späth, G.; Giordano, S.; Tommasini, C.; Bernardini, S.; De Luca, V.; Della Rocca, C.; Weiss, M.C.; Comoglio, P.M.; et al. Transgenic expression in the liver of truncated Met blocks apoptosis and permits immortalization of hepatocytes. *EMBO J.* **1997**, *16*, 495–503. [CrossRef] [PubMed]
12. Clavijo-Cornejo, D.; Enriquez-Cortina, C.; López-Reyes, A.; Domínguez-Pérez, M.; Nuño, N.; Domínguez-Meraz, M.; Bucio, L.; Souza, V.; Factor, V.M.; Thorgeirsson, S.S.; et al. Biphasic regulation of the NADPH oxidase by HGF/c-Met signaling pathway in primary mouse hepatocytes. *Biochimie* **2013**, *95*, 1177–1184. [CrossRef] [PubMed]
13. Gómez-Quiroz, L.E.; Factor, V.M.; Kaposi-Novak, P.; Coulouarn, C.; Conner, E.A.; Thorgeirsson, S.S. Hepatocyte-specific c-Met Deletion Disrupts Redox Homeostasis and Sensitizes to Fas-mediated Apoptosis. *J. Biol. Chem.* **2008**, *283*, 14581–14589. [CrossRef]
14. Gómez-Quiroz, L.; Gutiérrez-Ruiz, M.; Marquardt, J.; Factor, V.; Thorgeirsson, S. Redox regulation by HGF/c-Met in liver disease. In *Liver Pathophysiology*; Elsevier: Amsterdam, The Netherlands, 2017; pp. 375–387.
15. Issitt, T.; Bosseboeuf, E.; De Winter, N.; Dufton, N.; Gestri, G.; Senatore, V.; Chikh, A.; Randi, A.M.; Raimondi, C. Neuropilin-1 controls endothelial homeostasis by regulating mitochondrial function and iron-dependent oxidative stress. *iScience* **2018**, *11*, 205–223. [CrossRef]
16. Shalini, S.; Nikolic, A.; Wilson, C.H.; Puccini, J.; Sladojevic, N.; Finnie, J.; Dorstyn, L.; Kumar, S. Caspase-2 deficiency accelerates chemically induced liver cancer in mice. *Cell Death Differ.* **2016**, *23*, 1727–1736. [CrossRef] [PubMed]
17. Mantovani, A.; Allavena, P.; Sica, A.; Balkwill, F. Cancer-related inflammation. *Nature* **2008**, *454*, 436–444. [CrossRef]

18. Amicone, L.; Terradillos, O.; Calvo, L.; Costabile, B.; Cicchini, C.; Della Rocca, C.; Lozupone, F.; Piacentini, M.; Buendia, M.A.; Tripodi, M. Synergy between truncated c-Met (cyto-Met) and c-Myc in liver oncogenesis: Importance of TGF-β signalling in the control of liver homeostasis and transformation. *Oncogene* **2002**, *21*, 1335–1345. [CrossRef]
19. Pello, O.M.; De Pizzol, M.; Mirolo, M.; Soucek, L.; Zammataro, L.; Amabile, A.; Doni, A.; Nebuloni, M.; Swigart, L.B.; Evan, G.I.; et al. Role of c-MYC in alternative activation of human macrophages and tumor-associated macrophage biology. *Blood* **2012**, *119*, 411–421. [CrossRef]
20. Maksymchuk, O.; Shysh, A.; Kotliarova, A. Quercetin inhibits the expression of MYC and CYP2E1 and reduces oxidative stress in the myocardium of spontaneously hypertensive rats. *Acta Biochim. Pol.* **2023**, *70*, 199–204. [CrossRef]
21. Jia, W.-T.; Xiang, S.; Zhang, J.-B.; Yuan, J.-Y.; Wang, Y.-Q.; Liang, S.-F.; Lin, W.-F.; Zhai, X.-F.; Shang, Y.; Ling, C.-Q.; et al. Jiedu recipe, a compound Chinese herbal medicine, suppresses hepatocellular carcinoma metastasis by inhibiting the release of tumor-derived exosomes in a hypoxic microenvironment. *J. Integr. Med.* **2024**, *22*, 696–708. [CrossRef]
22. D'artista, L.; Moschopoulou, A.A.; Barozzi, I.; Craig, A.J.; Seehawer, M.; Herrmann, L.; Minnich, M.; Kang, T.-W.; Rist, E.; Henning, M.; et al. MYC determines lineage commitment in KRAS-driven primary liver cancer development. *J. Hepatol.* **2023**, *79*, 141–149. [CrossRef] [PubMed]